

Seismic wave propagation in anisotropic ice: Part I. Elasticity tensor and derived quantities from ice-core properties

A. Diez^{1,2,*} and O. Eisen¹

¹Alfred Wegener Institute Helmholtz Centre for Polar and Marine Research, Bremerhaven,
Germany

²Karlsruhe Institute of Technology, Karlsruhe, Germany

*now at: Scripps Institution of Oceanography, University of California, San Diego, USA

Correspondence to: A. Diez
(adiez@ucsd.edu)

Abstract. A preferred orientation of the anisotropic ice crystals influences the viscosity of the ice bulk and the dynamic behaviour of glaciers and ice sheets. Knowledge about the distribution of crystal anisotropy is mainly provided by crystal orientation fabric (COF) data from ice cores. However, the developed anisotropic fabric does not only influence the flow behaviour of ice, but also the propagation of seismic waves. Two effects are important: (i) sudden changes in COF lead to englacial reflections and (ii) the anisotropic fabric induces an angle dependency on the seismic velocities and, thus, recorded traveltimes. A framework is presented here to connect COF data from ice-cores with the elasticity tensor to determine seismic velocities and reflection coefficients for cone and girdle fabrics. We connect the microscopic anisotropy of the crystals with the macroscopic anisotropy of the ice mass, observable with seismic methods. Elasticity tensors for different fabrics are calculated and used to investigate the influence of the anisotropic ice fabric on seismic velocities and reflection coefficients, englacially as well as for the ice–bed contact. Hence, it is possible to remotely determine the bulk ice anisotropy.

1 Introduction

Understanding the dynamic properties of glaciers and ice sheets is one important step to determine past and future behaviour of ice masses. One essential part is to increase our knowledge of the flow of the ice itself. When the ice mass is frozen to the base its flow is primarily determined by internal deformation. The degree thereof is governed by the viscosity (or the inverse of softness) of ice. The viscosity depends on different factors, such as temperature, impurity content and the orientation of the anisotropic ice crystals (Cuffey and Paterson, 2010).

Ice is a hexagonal crystal (ice Ih) under natural conditions on earth. These ice crystals can align in specific directions in response to the stresses within an ice mass. A preferred orientation of the ice crystals causes the complete fabric to be anisotropic, in contrast to a random distribution of the ice crystals where the ice is isotropic on the macroscopic scale. This fabric anisotropy influences the viscosity of the ice. The shear strength is several orders of magnitude smaller perpendicular to the ice crystal's c-axis than parallel to it, as shown in laboratory studies (Ashby and Duval, 1985; Cuffey and Paterson, 2010).

The influence of anisotropic ice fabric on the flow behaviour of ice can directly be observed in radar profiles from ice domes. At ice domes and divides a prominent feature of flow conditions is a Raymond bump (Raymond, 1983; Martín et al., 2009b). As ice is a non-Newtonian fluid, it is softer and deforms more easily on the flanks of the ice dome or divide due to the higher deviatoric stress there compared to the centre of the dome. Thus, the vertical flow is slower at the dome itself than on the flanks. This leads to an apparent upwarping of the isochronous layers. The development and influence of anisotropic fabric on the flow of ice at divides and the effects on the development of Raymond bumps were investigated by, for instance, Pettit et al. (2007) and Martín et al. (2009a). At ice divides features like double bumps and synclines are observed (Drews et al., 2013), next to single bumps. Martín et al. (2009a) could reproduce these double bumps and synclines by including anisotropic rheology in a full-Stokes model. Hence, they are presently considered a direct evidence of the existence of developed anisotropic fabric.

A second prominent feature in radar data is the basal layer. Before the advent of multi-static, phase-sensitive radar systems, the basal layer has usually been observed only as an echo-free zone (EFZ). The onset of it was connected to the appearance of folds in ice cores on a centimetre scale (Drews et al., 2009). Considerable progress in radar imaging over the last decade make it now possible to image the very bottom layer of ice sheets (Bell et al., 2011; NEEM community members, 2013). The radar data show an often fuzzy basal layer, with a rough upper surface and considerably disturbed coherency of radar return power. The presence of the basal layer turns out to be widespread, especially in Antarctica (CREGIS, P. Gogineni, pers. comm. 2014). As the basal ice near the bed is subject to higher stresses and elevated temperatures than the ice above, it is the region where ice physical properties on the microscale change most rapidly (Faria et al., 2014b). These include changes in crystal orientation fabric (COF) properties and distribution.

With increasing computational power the incorporation of anisotropy into ice flow models becomes feasible in three dimensions as well as on regional scales. However, to include anisotropy in ice-flow modelling we need to understand the development and the distribution of the anisotropic fabric, i.e. we have to observe the variation in the COF distribution over depth, as well as the lateral extent. To extend our ability to determine the influence of these properties on ice flow and map them laterally beyond the 10 cm scale of ice cores, we have to advance our knowledge of the connection between microscale properties and macroscale features on the tenths to hundreds of meter-scale

observed with geophysical methods like radar and seismics.

60 The standard method to measure the COF distribution is to analyse thin sections from ice cores under polarized light. The anisotropy is then normally given in the form of the sample-averaging eigenvalues of the orientation tensor (Woodcock, 1977) in discrete depth intervals. From this we gain information about the local anisotropic conditions at the ice-core location. Radar data have also been used to analyse the changing COF over depth (Matsuoka et al., 2003; Fujita et al., 2006; Eisen et al., 2007; Matsuoka et al., 2009). The challenge in analysing radar data is to distinguish
65 the COF-induced reflections from the numerous conductivity-induced reflections. This distinction is important as conductivity-induced layers are isochrones; by following conductivity-induced reflections in radar data, layers of equal age can be followed over large distances. Currently, identifying and tracing undisturbed layering is one of the main methods being used to identify the location of a site for a potentially 1.5 Ma old ice core in East Antarctica (Fischer et al., 2013).

70 Further, the anisotropic fabric has an influence on the wave propagation of seismic waves. Hence, by analysing COF-induced reflections and traveltimes the anisotropic fabric on the macroscale can be determined. Not only the longitudinal (P) pressure waves can be analysed here for the anisotropic fabric but also the transverse waves, i.e. the horizontal (SH) and vertical (SV) shear wave. One of the first studies of seismic anisotropy in the context of ice crystal anisotropy was the PhD thesis
75 of Bennett (1968), who derived equations for the calculation of seismic velocities for solid cone and surface cone fabrics. He fitted curves to the slowness surface (inverse of the phase velocity) calculated from an elasticity tensor measured by means of ultrasonic sounding. This was applied to data from Dome C, Antarctica, by Blankenship and Bentley (1987). Bentley (1972) investigated the anisotropic ice fabric at Byrd Station, Antarctica, for which he used ultrasonic logging. To determine
80 the anisotropic seismic velocities for different cone fabrics, he calculated an average from the single crystal velocity for the encountered directions. This approach was used later by Gusmeroli et al. (2012) for analysing the crystal anisotropy from borehole sonic logging at Dome C, Antarctica.

These methods have one shortcoming. They limit the analysis of anisotropy of seismic waves to the analysis of the traveltimes, i.e. seismic velocities. The influence of anisotropy has not only
85 been observed in seismic velocities. Englacial reflections were also observed in seismic data from Antarctica (Horgan et al., 2011; Hofstede et al., 2013) and Greenland (Horgan et al., 2008). These reflections were interpreted as arising from an abrupt change in fabric orientation. However, to analyse the reflection signature and determine the actual change in COF, we first need an understanding of the reflection coefficient for changing incoming angles for the transition between different anisotropic
90 fabrics.

One way to improve the analysis of seismic data is to apply full waveform inversion algorithms, i.e. the analysis of the complete observed wave field and not only quantifiable characteristics such as reflection strength or traveltimes, which gains more and more importance in applied geophysics in general. If we want to be able to investigate and understand the influence of the anisotropic

95 ice fabric on the seismic wave field and develop ways to derive information from traveltimes and reflection signatures about different anisotropic ice fabrics from seismic data, we need to be able to derive the elasticity tensor for different COF distributions.

In this paper we extend the analysis of seismic velocities beyond cone fabrics and derive the elasticity tensor, which is necessary to describe the seismic wavefield in anisotropic media. The description of seismic wave propagation in anisotropic materials is based on the elasticity tensor, a 4th order tensor with 21 unknowns in the general case of anisotropy. If the elasticity tensor is known, seismic velocities, reflection coefficients or reflection angles, can be calculated. From ice core analysis one normally gains the COF eigenvalues describing the distribution of the crystal orientations. Hence, we first need a connection between the COF eigenvalues and the elasticity tensor.

We present a framework here to derive the elasticity tensor from the COF eigenvalues for cone as well as different girdle fabrics. We derive opening angles for the enveloping of the c-axis distribution from the COF eigenvalues. We then integrate using a monocrystal elasticity tensor for these derived distributions to obtain the elasticity tensor for the different anisotropic fabrics (Sect. 3). Based on these derived elasticity tensors we calculate seismic velocities and reflection coefficients for different c-axis distributions. As examples, we investigate the compressional wave velocity variations with increasing angle for different fabrics and the reflection coefficients for a change from isotropic to girdle fabric for compressional and shear waves. Further, we analyse the influence of anisotropy on the reflection signature of the ice–bed interface and discuss these results in Sect. 4. This is the first part of two companion papers. The calculations introduced here will be applied to ice-core and seismic data from Kohnen Station, Antarctica, in Part II, Diez et al. (2014, *subm.*).

2 Ice crystal anisotropy

The ice crystal is an anisotropic, hexagonal crystal with the basal plane perpendicular to the ice crystal's c-axis. Due to the existing stresses within glaciers and ice sheets these anisotropic ice crystals can be forced to align in one or several specific directions. In such cases the crystal's c-axis is oriented perpendicular to the main direction of stress (Cuffey and Paterson, 2010). Depending on the stress regime different COF distributions develop. Common stress regimes in glaciers are simple shear and uniaxial stress (Table 1). At ice domes simple shear can be observed, such that the ice crystals orient towards the vertical, i.e. cone distributions can be found, also called cluster distributions in mineralogy. At ice divides, with a main direction of extension and compression perpendicular to that, ice crystals tend to orient in one plane, i.e. in girdle distribution.

Different fabric distributions were discussed by Wallbrecher (1986), who classifies eight different fabric groups. Of these we will use the three most common fabrics observed in glacier ice in the following analysis of the influence of ice crystal anisotropy on seismic wave propagation: (i) the

130 cluster (or cone) distribution, (ii) the thick girdle distribution, and (iii) the partial girdle distribution. These distributions are shown in Table 1. The sketches (first row) show the enveloping of the specific c-axes distribution for the different fabrics. We will use the term cone fabric instead of cluster fabric hereinafter, as it is the more commonly used term in glaciology. The most extreme forms of anisotropy we can expect in ice are the isotropic fabric, with a uniform distribution of ice crystals, 135 and the vertical single maximum (VSM) fabric, where all ice crystals are oriented vertical. Note that the term 'lattice-preferred orientation (LPO)' is used as well in literature to refer to the orientation of the crystals (Faria et al., 2014a), in addition to COF.

2.1 Crystal orientation fabric measurements

The standard method of measuring COF distributions is by analysing thin sections from ice cores 140 under polarized light using an automatic fabric analyser (Wilson et al., 2003; Peternell et al., 2010). The c-axis orientation of each single crystal is determined and can be given as a unit vector (\mathbf{c}). These orientations can be presented in Schmidt plots, an equal-area projection of a sphere onto a plane, or as eigenvalues $\lambda_1, \lambda_2, \lambda_3$ of the weighted orientation tensor

$$145 \quad A_{ij} = W \sum_{l=1}^n (c_i c_j)_l, \quad \text{with } i, j = 1, 2, 3. \quad (1)$$

The number of grains is given by n and W is a weighting function, with weighting, e.g. by grain number ($W = 1/n$) or by area. The three eigenvalues, with $\lambda_1 \leq \lambda_2 \leq \lambda_3$ and $\sum \lambda_i = 1$, determine the extension of a rotation ellipsoid. The corresponding eigenvectors cannot be given when the orientation of the ice core within the borehole is not measured in geolocated directions. Hence, the 150 direction to which these eigenvalues apply is often unknown.

Another possibility to describe the anisotropic fabric is to calculate the spherical aperture from the orientation tensor. Hence, the c-axis distribution is given in the form of one opening angle for the enveloping cone (Wallbrecher, 1986). However, this limits the analysis of anisotropy to cone fabrics (Table 1).

155 2.2 Seismic anisotropy

The propagation of seismic waves is influenced by the anisotropic material, effecting, e.g. seismic velocities, reflection coefficients and reflection angles, among other properties. The propagation of wavefronts in the anisotropic case is no longer spherical. Figure 1 shows the anisotropic wavefront for a P-wave travelling in a VSM-fabric (red line) and the spherical wavefront for a P-wave in 160 isotropic ice fabric (dashed black line). For the anisotropic case group and phase velocity, as well as group angle θ and phase angle ϑ , are no longer the same. The group velocity determines the traveltime. The phase velocity vector is normal to the wavefront. Thus, the phase velocity and phase angle ϑ are needed for the calculation of reflection and transmission angles as well as reflection coefficients in anisotropic media.

165 For an anisotropic medium the linear relationship between tensors of stress σ_{mn} and strain τ_{mn} is described by Hooke's law

$$\sigma_{mn} = c_{mnop}\tau_{op}, \quad (2)$$

with the elasticity tensor c_{mnop} and $m, n, o, p = 1, 2, 3$. In the isotropic case these 81 components
 170 of the elasticity tensor can be reduced to the two well-known Lamé parameters. In the general anisotropic case, symmetry consideration of the strain and stress tensors apply, as well as thermodynamic considerations (Aki and Richards, 2002). Hence, the general anisotropic elasticity tensor consist of 21 independent components and is referred to as triclinic.

To determine seismic velocities in anisotropic media a solution for the wave equation needs to
 175 be found. Given here is the wave equation for homogeneous, linear elastic media, without external forces and with triclinic anisotropy

$$\rho \frac{\partial^2 u_m}{\partial t^2} - c_{mnop} \frac{\partial^2 u_o}{\partial x_n \partial x_p} = 0, \quad (3)$$

with ρ the density of the material, t time, the components u_m and u_o of the displacement vector \mathbf{u}
 180 and the different spatial directions x_n, x_p . Solving this equation leads to an eigenvalue problem, the Christoffel equation. For a detailed derivation see, e.g. Tsvankin (2001).

Finally, three non-trivial solutions exist for this eigenvalue problem, giving the three phase velocities and vectors for the quasi compressional (qP), the quasi vertical (qSV) and the quasi horizontal shear (qSH) wave. The phase vectors are orthogonal to each other. However, qP- and qSV-waves are
 185 coupled, so the waves are not necessarily pure longitudinal or shear waves outside of the symmetry planes. Therefore, they are additionally denoted as 'quasi' waves, i.e. qP-, qSV- and qSH-waves. As the following analyses are mostly within the symmetry planes, the waves will from now on be denoted as P-, SV- and SH-waves. Nevertheless, outside of the symmetry planes this term is not strictly correct.

190 To be able to find analytical solutions of the Christoffel matrix the anisotropic materials are distinguished by their different symmetries. Additionally, to simplify calculations with the elasticity tensor we will use the compressed Voigt notation (Voigt, 1910) for the elasticity tensor $c_{mnop} \rightarrow C_{ij}$. Therefore, the index combinations of mn and op are replaced by indices between 1 and 6 ($11 \equiv 1$, $22 \equiv 2$, $33 \equiv 3$, $23 \equiv 4$, $13 \equiv 5$, $12 \equiv 6$). Considering only certain symmetries reduces the unknowns
 195 of the elasticity tensor C_{ij} further. For the analysis of anisotropic ice we consider cone, thick and partial girdle fabric. The connection between the different fabric types and symmetry classes, i.e. seismic terminology for this fabric, can be found in Table 1. Partial girdle fabric is the fabric with the

lowest symmetry, corresponding to an orthorhombic medium, with 9 unknowns,

$$C_{ij} = \begin{pmatrix} C_{11} & C_{12} & C_{13} & 0 & 0 & 0 \\ C_{12} & C_{22} & C_{23} & 0 & 0 & 0 \\ C_{13} & C_{23} & C_{33} & 0 & 0 & 0 \\ 0 & 0 & 0 & C_{44} & 0 & 0 \\ 0 & 0 & 0 & 0 & C_{55} & 0 \\ 0 & 0 & 0 & 0 & 0 & C_{66} \end{pmatrix}. \quad (4)$$

200

In case of orthorhombic media three symmetry planes, i.e. orthogonal planes of mirror symmetry exist. The number of unknowns can be reduced further to five unknowns if transversely isotropic media exists, resulting in an anisotropy with a single axis of rotation symmetry. This is normally distinguished in vertical transversely isotropic (VTI) and horizontal transversely isotropic (HTI) media, with a vertical and horizontal axis of rotation symmetry, respectively. A vertical cone fabric, including VSM fabric, would be classified as VTI media while a thick girdle fabric as given in Table 1 would be classified as HTI media. This distinction is important for the calculation of seismic velocities and reflection coefficients as the calculation simplifies for wave propagation within symmetry planes of the anisotropic fabric (Sect. 4)

210 3 Calculation of elasticity tensor from COF eigenvalues

From the analysis of ice cores we determine the COF eigenvalues which describe the crystal anisotropy over depth. The propagation of seismic waves in anisotropic media can be calculated from the elasticity tensor. Hence, a relationship between the COF eigenvalues and the elasticity tensor is needed.

For the following derivation of the elasticity tensor we will use two opening angles for the description of the fabric that envelopes the c-axis distribution. Thus, we are able to take into account cone as well as girdle fabric distributions. We distinguish between an opening angle χ in x_1 -direction and an opening angle φ in x_2 -direction in a coordinate system where the x_3 -axis is pointing downwards (Table 1). These opening angles will be calculated from the COF eigenvalues.

The two opening angles determine the kind of fabric (Table 1). If the angles φ and χ are equal, the c-axis distribution is a cone distribution with the cone opening angle $\varphi = \chi$, i.e. it is a VTI media. The two extrema of this distribution are the uniform distributions, i.e. the isotropic case, and the VSM-fabric. All c-axes are oriented vertically in case of a VSM-fabric. The eigenvalues are $\lambda_1 = \lambda_2 = 0$ and $\lambda_3 = 1$ and the cone opening angle is 0° . The ice crystals are randomly oriented in case of isotropic fabric. The eigenvalues are then $\lambda_1 = \lambda_2 = \lambda_3 = 1/3$ and the cone opening angle is 90° . The thick girdle fabric is an HTI media: The c-axes are distributed between two planes with a certain distance, so that the opening angle φ in x_2 -direction is 90° and χ in x_1 -direction gives the thickness of the girdle. The partial girdle fabric, an orthorhombic media, is a distribution where all ice crystal c-axes are in one plane, but only within a slice of this plane, so that the opening angle χ

225

in x_1 -direction is 0° and φ in x_2 -direction gives the size of the slice within the plane. A girdle fabric
 230 with $\chi = 0^\circ$ and $\varphi = 90^\circ$ would correspond to the eigenvalues $\lambda_1 = 0$ and $\lambda_2 = \lambda_3 = 0.5$.

We will use a measured monocrystal elasticity tensor here to calculate the elasticity tensor for
 the different observed anisotropic fabrics in ice from the COF eigenvalues. For monocrystalline ice
 the components of the elasticity tensor have been previously measured by a number of authors with
 different methods. For the following calculations we use the elasticity tensor of Gammon et al.
 235 (1983) ($C_{11} = 13.93 \pm 0.04 \text{ GN m}^{-2}$; $C_{33} = 15.01 \pm 0.05 \text{ GN m}^{-2}$; $C_{55} = 3.01 \pm 0.01 \text{ GN m}^{-2}$;
 $C_{12} = 7.08 \pm 0.04 \text{ GN m}^{-2}$; $C_{13} = 5.77 \pm 0.02 \text{ GN m}^{-2}$). The c-axis of this ice crystal is oriented
 vertically here, parallel to the x_3 -direction (Table 1).

3.1 From COF eigenvalues to opening angles

When the COF eigenvalues are derived, the information on the fabric distribution is significantly re-
 240 duced, especially as the corresponding eigenvectors are normally unknown. Hence, it is not possible
 to determine the elasticity tensor with at least five unknowns directly from the three COF eigenval-
 ues. Therefore, we first subdivide the observed anisotropies into different fabric groups (cone, thick
 girdle and partial girdle fabric) by means of the eigenvalues. Afterwards, we determine their opening
 angles (Sect. 2.1).

245 To differentiate between cone and girdle fabric Woodcock (1977) suggests a logarithmic repre-
 sentation of the eigenvalues and classification by a slope

$$m = \frac{\ln(\lambda_3/\lambda_2)}{\ln(\lambda_2/\lambda_1)}. \quad (5)$$

The fabric is a cone fabric with $m > 1$ and a girdle fabric with $m < 1$. However, we want to put a
 250 stronger tendency towards a classification of the fabric as cone fabric. In the seismic sense a cone
 fabric is a VTI media. It is easier to calculate velocities and reflection coefficients for VTI media
 compared to girdle fabric, i.e. HTI media. Hence, we use a threshold value to distinguish between
 cone and girdle fabric. If $\lambda_1 \leq 0.1$ and $\lambda_2 \geq 0.2$ the fabric is classified as girdle fabric, everything
 else is classified as cone fabric. Additionally, we set a threshold to distinguish within the girdle
 255 fabric between partial and thick girdle fabric. If $\lambda_1 \leq 0.05$ the fabric is classified as partial girdle,
 otherwise as thick girdle. By distinguishing between these fabrics we know that $\varphi = \chi$ for the cone
 fabric, $\varphi = 90^\circ$ for the thick girdle fabric and $\chi = 0^\circ$ for the partial girdle fabric (Table 1).

In the next step the remaining, unknown opening angle for the different fabrics needs to be cal-
 culated from the eigenvalues, i.e. φ for the cone fabric, χ for the thick girdle fabric and φ for the
 260 partial girdle fabric. Wallbrecher (1986) for instance connects the opening angle φ of a cone fabric
 with the eigenvalue λ_3 by $\lambda_3 = 1 - 2/3 \sin^2 \varphi$. To verify this calculation we determine the eigenval-
 ues for cone angles between 0 and 90° . In total 10000 randomly distributed vectors were created,
 giving a random distribution of c-axes. For each cone angle the vectors within this cone angle were
 selected. The eigenvalues for this cone angle were then calculated from these vectors. The process

265 was repeated 100 times for each cone angle φ . The calculated $\lambda_3(\varphi)$ values from the equation given
 by Wallbrecher (1986) differ by up to 15° for φ . For a more precise connection of λ_3 and φ than
 available from literature a 4th-order polynomial was fitted to the λ_3 - φ values (App. A1). The same
 was done for the calculation of χ from λ_1 for thick girdle fabrics, as well as for the calculation of
 φ from λ_3 for partial girdle fabrics (App. A1). The orientation of the girdle is normally not known.
 270 Thus, the azimuth ψ (Fig. 2) of the girdle fabric cannot be determined from the eigenvalues. This is
 only possible if the eigenvector belonging to the eigenvalue λ_1 , the normal to the plane of the girdle,
 is known in geolocated directions. Hence, in the following we normally assume girdle fabrics to be
 orientated as HTI media with the azimuth $\psi = 0^\circ$ for the calculation of the elasticity tensor.

3.2 From opening angles to the elasticity tensor

275 The elasticity tensor of the polycrystal can now be derived using the measured elasticity tensor for
 a single ice crystal and the derived angles χ and φ . For the calculation of the polycrystal elasticity
 tensor C_{ij} we follow the idea of Nanthikesan and Sunder (1994). They use the concept of the Voigt
 (1910) and Reuss (1929) bounds. This concept was developed to calculate the elasticity tensor of
 isotropic polycrystals, containing different crystals. This concept is generalized by Nanthikesan and
 280 Sunder (1994) to calculate the elasticity tensor for anisotropic fabrics.

Voigt (1910) assumed that the strain on the polycrystal introduces the same uniform strain in all
 monocrystals. On the contrary, Reuss (1929) assumed that the stress on the polycrystal introduces
 the same uniform stress in all monocrystals. To calculate the elasticity tensor of the polycrystal with
 the Voigt (1910) assumption one has to average over the elasticity tensor C_{ij}^m of the monocrystal
 285 (superscript m). In case of the Reuss (1929) assumption, the compliance tensor of the polycrystal is
 calculated by averaging over the compliance tensor S_{ij}^m of the single crystals. The compliance tensor
 of a crystal is the inverse of the elasticity tensor, here given in terms of Hooke's law (Eq. (2)):

$$\tau_{mn} = s_{mnop}\sigma_{op}. \quad (6)$$

290 For the inversion of elasticity to compliance tensor and vice versa see, e.g. Bower (2010). The
 method of Voigt (1910) and Reuss (1929) is an approximation of the elasticity tensor due to violation
 of local equilibrium and compatibility conditions across grain boundaries, respectively. Hill (1952)
 showed that the concepts of Voigt (1910) and of Reuss (1929) give the upper and lower limit for the
 elastic moduli of the polycrystal C_{ij} , referred to as Voigt–Reuss bounds,

$$295 \quad C_{ij}^R \leq C_{ij} \leq C_{ij}^V, \quad (7)$$

where the superscripts R and V denote Reuss (1929) and Voigt (1910) calculation, respectively.

To obtain the elasticity tensor of the anisotropic polycrystal C_{ij} from the elasticity tensor of the
 monocrystal C_{ij}^m with different orientations one has to integrate the elasticity tensor $\tilde{C}_{ij}^m(\phi)$ with a
 300 probability density function $F(\phi)$ for the different c-axes orientations, where ϕ gives the minimum

(ϕ_1) and maximum (ϕ_2) extent of the c-axes in the plane. This plane is perpendicular to the corresponding rotation axis, so that the elasticity tensor $\tilde{C}_{ij}^m(\phi)$ is determined from the monocystal elasticity tensor C_{ij}^m using the rotation matrix R_{ij}^C

$$305 \quad \tilde{C}_{ij}^m(\phi) = (R_{ij}^C)^T C_{ij}^m R_{ij}^C. \quad (8)$$

The rotation matrices R_{ij}^C for the different directions in space are given in App. A2, $(R_{ij}^C)^T$ is the transpose of R_{ij}^C . The same applies for the calculation of the monocystal compliance tensor depending on ϕ , with

$$310 \quad \tilde{S}_{ij}^m(\phi) = (R_{ij}^S)^T S_{ij}^m R_{ij}^S. \quad (9)$$

with the rotation matrix R_{ij}^S for the compliance tensor (App. A2) and its transpose $(R_{ij}^S)^T$. For a uniform distribution of the c-axis orientations the probability density function can be given by

$$F(\phi) = \frac{1}{\phi_2 - \phi_1} \quad \text{for } \phi_1 \leq \phi \leq \phi_2 \quad (10)$$

$$315 \quad = 0 \quad \text{text for } \phi_2 \leq \phi \leq \pi; -\pi \leq \phi \leq \phi_1, \quad (11)$$

which is symmetric around the main orientation, so that $\phi_1 = -\phi_0$ and $\phi_2 = +\phi_0$. The elasticity tensor of the anisotropic polycrystal is then calculated by

$$C_{ij} = \frac{1}{2\phi_0} \int_{-\phi_0}^{+\phi_0} \tilde{C}_{ij}^m(\phi) d\phi, \quad (12)$$

320 and the compliance tensor is calculated by

$$S_{ij} = \frac{1}{2\phi_0} \int_{-\phi_0}^{+\phi_0} \tilde{S}_{ij}^m(\phi) d\phi. \quad (13)$$

After considering the orthorhombic symmetry and some rearranging of the results of Eqs. (12) and (13) the components of the elasticity tensor and compliance tensor of a polycrystal can be expressed in compact form. The results are different for c-axes distributions in the different spatial directions x_1 , x_2 and x_3 . As an example, the equations for the elasticity and compliance tensor for a rotation around the x_1 direction are given in App. A3. This would correspond to a c-axis distribution in the $[x_2, x_3]$ -plane. The equations for rotation around the x_2 -axis and the x_3 -axis can equally be derived from Eqs. 12 and 13.

330 The different rotation directions to calculate the polycrystal elasticity tensor C_{ij} from a vertically oriented monocystal elasticity tensor C_{ij}^m for cone, thick girdle and partial girdle fabric are listed in Table 2. They are also valid for the compliance tensor. For the calculation of the elasticity tensor of a partial girdle (Table 1) the elasticity tensor of the monocystal C_{ij}^m is rotated around the x_1 -axis with the opening angle of the partial girdle in x_2 -direction (φ). The elasticity tensor is then calculated

335 using Eq. (A12) with $\phi_0 = \varphi$. For a thick girdle $\varphi = 90^\circ$ to gain a full girdle in the $[x_2, x_3]$ -plane
in the first step. In a second step this elasticity tensor obtained for a full girdle is then rotated
around the x_2 -axis with $\phi_0 = \chi$. For cone fabrics with different opening angles the elasticity tensor
of a monocrystal is rotated around the x_1 -axis (Eq. (A12)) in a first step using the cone opening
angle ($\phi_0 = \varphi = \chi$) and, afterwards, the obtained elasticity tensor is rotated around the x_3 -axis with
340 $\phi_0 = 90^\circ$.

3.3 Limitations of the method

Nanthikesan and Sunder (1994) developed the approach to calculate the polycrystal elasticity tensor
from the monocrystal elasticity tensors for, what they call, S1 (vertical single maximum), S2 (hor-
zontal girdle) and S3 (horizontal partial girdle) ice for given opening angles. They found that the
345 Voigt–Reuss bounds for these fabrics are within 4.2% of each other and concluded from this that
either calculation, by means of the elasticity tensor (Eq. (12)) or compliance tensor (Eq. (13)), can
be used to calculate the elasticity tensor of the polycrystal. We use the approach of Nanthikesan and
Sunder (1994) not only for the calculation of partial girdle fabrics but also for the calculation of the
polycrystal elasticity tensor of thick girdle and cone fabrics.

350 By comparing the individual components of the elasticity tensor derived following Voigt (1910)
(Eq. (12)) with those of the elasticity tensor derived following Reuss (1929) (Eq. (13) and taking the
inverse of the compliance tensor) the largest difference of 4.2% for all the investigated fabrics can be
found for the components C_{44} (S_{44}) of a partial girdle with an opening angle of 50° and 90° . Thus,
for all fabrics in this study, the Voigt–Reuss bounds are within 4.2% of each other and we follow
355 Nanthikesan and Sunder (1994) in their argumentation that either calculation can be used. However,
using the Voigt (1910) calculation no extra step in the calculation is needed to invert the compliance
tensor. Therefore, for all further calculations the approach by Voigt (1910) is used (Eq. (12)).

To be able to calculate the opening angles from the COF eigenvalues the fabrics are classified into
the different fabric groups based on their eigenvalues: cone, thick girdle and partial girdle fabric
360 (Table 1). This classification introduces artificial discontinuities in the velocity profile over depth,
calculated from an ice core. These discontinuities only reflect the calculation method and no sudden
changes in the prevailing fabric (Part II, Diez et al., 2014, *subm.*). This limitation, introduced by
the classification of the different fabric groups, could be overcome by calculating the opening angles
directly from the derived c -axis vectors. Another possibility would be to calculate the elasticity
365 tensor using the orientation distribution function (ODF), e.g. using the open source software METX
(Mainprice et al., 2011). The calculation of the elasticity tensor in this software is likewise based
on Voigt–Reuss bounds, as is done in this study. However, in glaciology the fabric distribution is
normally presented in the compact form of the COF eigenvalues. With the here presented framework
the information of the eigenvalues can directly be used for the calculation of the elasticity tensor,
370 without further information. To enable direct applicability of our method to existing ice-core data

sets, we except the limitations of our approach for the sake of ease of use.

For the calculation of the anisotropic polycrystal from the monocrystal neither grain size nor grain boundaries are considered. Elvin (1996) modelled the number of grains that are necessary to homogenize the elastic properties of polycrystalline ice and found, that at least 230 grains are needed
375 for girdle fabric (S2 ice). This number of ice crystals should be reached with seismic waves in ice of around 300 Hz, i.e. a wavelength of more than 10 m and ice crystals with ≤ 0.1 m diameter on average. Additionally, Elvin (1996) computed two cases, with and without grain boundary sliding and found a difference of up to 25% in Young's modulus and Poisson ratio. In absence of grain-boundary sliding the anisotropy mainly defines the elastic behaviour. Otherwise, grain shape and
380 grain-boundary sliding become important as well. A certain mistake is, thus, made for the calculation of the polycrystal by only considering the influence of the anisotropy of the monocrystal.

The resultant polycrystal elasticity tensors depends of course on the choice of the monocrystal elasticity tensor. Different authors measured (Jona and Scherrer, 1952; Green and Mackinnen, 1956; Bass et al., 1957; Brockamp and Querfurth, 1964; Bennett, 1968; Dantl, 1968; Gammon et al., 1983)
385 and calculated (Penny, 1948) the monocrystal elasticity tensor. A comparison of the different elasticity tensors used can be found in Part II (Diez et al., 2014, *subm.*). There we investigate results of a vertical seismic profiling survey in comparison to quantities from measured COF eigenvalues. We find the best agreement between measured and calculated velocities using the monocrystal elasticity tensor of Gammon et al. (1983) for the derivation of the polycrystal elasticity tensor.

390 **4 Seismic velocities and reflection coefficients in anisotropic ice**

From the derived elasticity tensor we can now calculate velocities and reflection coefficients. Many approximations as well as exact solutions exist for the calculation of velocities and reflection coefficients for different anisotropic fabrics. They are mostly limited to certain symmetries.

In the case of velocities, most studies have been performed on VTI media (e.g. Daley and Heron,
395 1977). These solutions are still valid within the symmetry planes of HTI media. To be able to calculate seismic velocities for the different fabrics in ice we will use a calculation of velocities for orthorhombic media derived by Daley and Krebes (2004) (Sect. 4.1). We compare our calculated velocities, based on the derived elasticity tensor, with the well known velocities for a solid cone that were derived by Bennett (1968) (Sect. 4.2).

400 For the calculation of the reflection coefficient we use exact (Graebner, 1992) as well as approximate (Rüger, 1997; Zillmer et al., 1998b) calculations (Sect. 4.3). We show the reflection coefficients for an abrupt change from isotropic to partial girdle fabric here as an example (Sect. 4.4). Additionally, we investigate the influence on the reflection signature of an anisotropic ice mass above the base (Sect. 4.5).

405 4.1 Velocities in orthorhombic media

For the special case of wave propagation in ice with a developed cone fabric anisotropy Bennett (1968) derived equations of the slowness surface for P-, SV- and SH-waves. The phase velocities are given by the inverse of the slowness surface. To calculate the slowness surface over different angles Bennett (1968) first derived the elasticity tensor from single natural ice crystals by measurements of
 410 ultrasonic pulses of 600 kHz. With the derived equations, velocities for different incoming angles ϑ in dependence of the cone opening angle φ can be calculated. It is not possible to calculate velocities for girdle fabrics with this approach.

Using the derived elasticity tensor we are now able to calculate velocities for different COF distributions. We use the equations derived by Daley and Krebes (2004) for the calculation of phase
 415 velocities v_{ph} (v_{p} , v_{sv} , v_{sh}) as a function of the phase angle ϑ for orthorhombic media as given in App. B1 (Eqs. (B1)–(B3)).

From these phase velocities we have to calculate the group velocities for the calculation of travel-times. The calculation of the group velocity vector \mathbf{v}_{g} can be found, e.g. in Rommel and Tsvankin (2000) and Tsvankin (2001). If the propagation of the seismic wave is within symmetry planes of
 420 the anisotropic fabric the group velocity and group angle can be given in compact form. The group velocity v_{g} is then calculated from the phase velocity v_{ph} by

$$v_{\text{g}} = v_{\text{ph}} \sqrt{1 + \left(\frac{1}{v_{\text{ph}}} \frac{\partial v_{\text{ph}}}{\partial \vartheta} \right)^2} \quad (14)$$

with the group angle θ in the symmetry plane defined by

$$425 \tan \theta = \frac{\tan \vartheta + \frac{1}{v_{\text{ph}}} \frac{\partial v_{\text{ph}}}{\partial \vartheta}}{1 - \frac{1}{v_{\text{ph}}} \frac{\partial v_{\text{ph}}}{\partial \vartheta} \tan \vartheta}. \quad (15)$$

Outside the symmetry planes of, e.g. HTI media, all components of the group velocity vector \mathbf{v}_{g} have to be considered (App. B1).

Figure 3 shows the phase (dashed curves) and group velocities (solid curves) as a function of the
 430 corresponding phase ϑ and group angle θ of P- (red), SV- (light blue) and SH-wave (blue) for a VSM-fabric. The largest difference between phase and group velocity can be observed for the SV-wave (light blue curves) with a triplication in the group velocity for group angles of 43–47°. Here three different velocities are given for each angle. Due to the small spread of these velocities, we do not expect that this triplication is of relevance for applications given the current day accuracy of
 435 measurements. The SV-velocity is largest for 45° incoming angle (phase as well as group angle) with 2180 m/s, decreasing for 0° and 90° to 1810 m/s. Variations for the SH-wave are rather small with velocities increasing between 0° and 90° from 1810 m/s to 1930 m/s, i.e. 6%. The P-wave velocity has a minimum at ~51° incoming angle with 3770 m/s. The highest wave speed is observed for waves parallel to the c-axis of an ice crystal (0° incoming angle) with 4040 m/s and 150 m/s (4%)
 440 slower perpendicular to it.

4.2 Velocities for anisotropic ice

By deriving the elasticity tensor for different fabrics the group and phase velocities of P-, SH- and SV-wave for these fabrics can now be calculated. Figure 4 show the P-wave phase velocity for different cone and girdle fabrics calculated with the equations given in Daley and Krebs (2004) and the equations derived by Bennett (1968) for a solid cone. The phase velocity for the SH- and SV-wave as well as the corresponding group velocities can be displayed accordingly (Diez, 2013). Here, we will limit our analysis to P-waves. However, with the derived elasticity tensor SH- and SV-wave velocities can just as well be investigated and the effect of S-wave splitting can be analysed.

Figure 4d shows the velocities calculated from the equations derived by Bennett (1968) for a solid cone from the elasticity tensor he measured at -10°C . These velocities were corrected to -16°C (Kohnen, 1974; Gammon et al., 1983) for better comparison with the other results, where we use the elasticity tensor of Gammon et al. (1983) measured at -16°C . The other subfigures are phase velocities calculated with Eq. (12) from an elasticity tensor derived following the steps in Table 2 with the elasticity tensor measured by Gammon et al. (1983). The top row (Fig. 4) shows velocities for cone fabric (subfigure a: VTI) as well as partial girdle fabric (b: HTI) and thick girdle fabric (c: HTI) in the $[x_2, x_3]$ -plane, while the bottom row shows velocities for cone fabric calculated following Bennett (1968) (d: VTI) as well as partial girdle fabric (f: $\psi = 90^{\circ}$) and thick girdle fabric (e: $\psi = 90^{\circ}$) in the $[x_1, x_3]$ -plane.

The partial girdle ($\chi = 0^{\circ}$, Fig. 4, b, e) with $\varphi = 90^{\circ}$ displays the same fabric as the thick girdle ($\varphi = 90^{\circ}$, Fig. 4, c, f) with $\chi = 0^{\circ}$. The same applies to the cone fabric with an opening angle of 90° (Fig. 4, a, d) as well as the thick girdle fabric ($\varphi = 90^{\circ}$) with $\chi = 90^{\circ}$ (Fig. 4, c, f), both showing isotropic c-axes distribution. Apart from Bennett's velocities, these velocities for the isotropic state (Fig. 4, a, c, f) are obviously not isotropic. Slight variations still exist for these velocities with increasing incoming angle. This is due to artefacts that seem to appear from the derivation of the elasticity tensor for the isotropic state using the single crystal elasticity tensor.

It should also be noted, that for a thick girdle with $\varphi = \chi = 90^{\circ}$ the variations over the incoming angle are just reversed to that of the cone fabric with opening angle $\varphi = \chi = 90^{\circ}$. This reflects the difference in the calculation of the elasticity tensor from cone fabric and girdle fabric. While a girdle with $\varphi = 90^{\circ}$ ($\chi = 0^{\circ}$) is calculated in the first step for both fabrics (Table 2) by integration with rotation around the x_1 -axis, the second step is an integration with rotation around the x_3 -axis for the cone fabric and around the x_2 -axis for the thick girdle fabric.

The higher velocities calculated with the equations of Bennett (1968) (Fig. 4, d) are due to the difference in the elasticity tensor, as the elasticity tensor derived by Gammon et al. (1983) was used for the calculation in all of the other subfigures (Fig. 4, a–c, e, f). The Bennett (1968) calculation exhibits an isotropic state for $\varphi = \chi = 90^{\circ}$. However, this is only possible as Bennett (1968) used fitted curves for the derivation of the slowness surface.

4.3 Reflection coefficients

The calculation of reflection coefficients for different incoming angles is already rather complicated for layered isotropic media given by the Zoeppritz equations (e.g. Aki and Richards, 2002). In the case of anisotropic media most of the studies have been done for VTI media (Keith and Crampin, 1977; Daley and Heron, 1977) and in terms of Thomsen parameters (Thomsen, 1993). A comprehensive overview of the different calculations of reflection coefficients for VTI and HTI media is given by Rüger (2002).

In the following, we use equations derived by Zillmer et al. (1997) by means of perturbation theory for the calculation of englacial reflection horizons. These equations for general anisotropy were simplified by Zillmer et al. (1998a) for weak contrast interfaces. They are, thus, especially practical for the reflection coefficients in ice. For the isotropic reference values the elasticity tensor for isotropic ice can be used and no average needs to be taken over different materials. The reflection coefficients for the anisotropic material are then calculated as perturbations of the isotropic ice fabric. Thus, reflection coefficients for P-, SV- and SH-waves are obtained. The equations for the calculation of reflection coefficients are given in App. B2. The R_{shsh} and R_{svsv} reflection coefficients are restricted to a symmetry plane of the layered medium. The indices give the polarisation of the incoming and reflected wave, e.g. R_{pp} is the reflection coefficient for an incoming P-wave, reflected as P-wave, equivalent for R_{shsh} and R_{svsv} .

To calculate the P-wave reflection coefficient for the bed reflector with an overlaying cone fabric, i.e. VTI media, we use the equations given by Thomsen (1993), that were further developed by Rüger (1997). Exact solutions for VTI media are, for example, given by Keith and Crampin (1977) or Graebner (1992).

4.4 Reflection coefficients for anisotropic ice

With the equations given in App. B2 (Zillmer et al., 1998a) reflection coefficients can be calculated for interfaces between different fabrics. Figure 5 shows as an example the R_{pp} , R_{shsh} and R_{svsv} reflection coefficient for the transition at a layer interface from an isotropic fabric to a partial girdle fabric, both for HTI media ($\psi = 0^\circ$) and with an azimuth of $\psi = 90^\circ$.

The reflection coefficients are given for angles of incidence between 0° and 60° . This has two reasons. Firstly, most seismic surveys do not exceed an incoming angle of 60° as this already corresponds to a large offset compared to the probed depth. Secondly and more important, the calculation of the reflection coefficients using Eqs. (B12)–(B13) is not exact. Instead, the error increases with increasing incoming angle.

The largest magnitude of reflection coefficients can be observed for the SVSV-reflection (Fig. 5). However, the reflection coefficients are ≤ 0.1 for all fabric combinations shown here. Most significantly, for the PP-reflection the reflection coefficients between different anisotropic fabrics are

small. The PP-reflection between, for example isotropic and VSM-fabric ice for normal incidence is < 0.02 . For comparison the reflection coefficient between isotropic and lithified sediments (Fig. 6) is ~ 0.4 . Hence, reflection coefficients at the ice–bed interface are an order of magnitude larger than reflection coefficients for the transition between different anisotropic fabrics. To be able to observe englacial seismic reflections, abrupt changes (i.e. within a wavelength) with significant variations in the orientation of the ice crystals are needed. Such englacial reflections have been observed in data from Greenland (Horgan et al., 2008), Antarctica (Horgan et al., 2011; Hofstede et al., 2013) and also in the Swiss Alps (Polom et al., 2014; Diez et al., 2013). These reflections can indicate a change in the fabric. However, the investigation of reflection signatures (amplitude versus offset, AVO) of englacial reflectors is difficult due to the small reflection coefficients, and the small range they cover with changing incoming angle.

For englacial reflections caused by changing COF the variations in the reflection coefficient with offset are very small: The PP-reflection coefficient for the transition from isotropic to VSM-fabric ($\varphi = 0^\circ$, Fig. 5) from 0° to 60° is between 0.019 and 0.036. To put these values in perspective we consider error bars for reflection coefficients as determined for ice–bed interfaces. It cannot be expected that the error bars for measuring the reflection coefficient of englacial reflections would be smaller than those given for the bed reflection coefficients. Peters et al. (2008) analysed the reflection amplitude for the ice bed interface from a survey near the South Pole. For the reflection coefficients they derive from the seismic data they give error bars of ± 0.04 , with increasing error bars for decreasing incoming angles, limited by ± 0.2 . The change in the reflection coefficient with offset for englacial reflection that we calculate is smaller than the given error bars. Thus, it is not possible to derive information about the anisotropic fabric from englacial reflections using AVO analysis at the moment. To be able to derive fabric information from AVO analysis the error in determining the reflection coefficient from seismic data needs to be reduced, e.g. better shooting techniques to reduce the signal-to-noise ratio (SNR) in the data or a better understanding of the source amplitude as well as the damping of seismic waves in ice.

4.5 Reflection coefficients for ice–bed interface

Of special interest is the determination of the properties of the ice–bed interface from seismic data. It is possible to determine the bed properties below an ice sheet or glacier by analysing the normal incident reflection coefficient (e.g. Smith, 2007) or by AVO analysis (Anandakrishnan, 2003; Peters et al., 2008). Fig. 6 shows reflection coefficients for the transition from isotropic and anisotropic (VSM-fabric) ice to different possible bed properties (Table 3). The values for density, P-wave and S-wave velocity, for the different bed scenarios and the isotropic ice, are taken from Peters et al. (2008). For the anisotropic VSM-fabric the elasticity tensor of Gammon et al. (1983) is used.

Exact solutions are calculated using the equations given by Graebner (1992), with corrections by Ruger (2002). Their equations were used to calculate the exact reflection coefficients for the

isotropic ice above the bed (solid lines) and for the anisotropic ice above the bed (dashed lines) shown in Fig. 6. The approximate reflection coefficients for the isotropic ice above the bed (dotted lines) are calculated using equations given in Aki and Richards (2002). The approximate reflection coefficients for the VSM-fabric above the bed (dashed-dotted lines) are calculated using equations given in Rüger (1997).

The differences between the isotropic (solid lines) and anisotropic reflection coefficients (dashed lines) are small (≤ 0.04) for the exact solutions. The approximate calculations fit well to the exact solutions up to a group angle of about 30° , with differences of the same order as isotropic to anisotropic variations. However, differences between exact and approximate reflection coefficients become large for increasing phase angle ($\geq 30^\circ$). Thus, errors introduced by using approximate calculations for the reflection coefficients are larger than the effect of anisotropic ice fabric above the bed.

The observable differences of reflection coefficients for an isotropic and a VSM-fabric overburden are ≤ 0.04 , i.e. smaller than the smallest error bars given by Peters et al. (2008) (Sect. 4.4). The VSM-fabric is the strongest anisotropy to be expected in ice. If an anisotropic layer exists above the bed, it yields a different reflection coefficient compared to the case of the isotropic ice overburden. However, the difference between the isotropic overburden reflection coefficient and the anisotropic overburden reflection coefficient is within the range of the error bars given by Peters et al. (2008). Thus, the anisotropic fabric will not have a measurable influence on the analysis of the bed properties by means of the AVO method, given the current degree of data accuracy and SNR.

5 Conclusions

We presented an approach to derive the ice elasticity tensor, required for the calculation of seismic wave propagation in anisotropic material, from the COF eigenvalues derived from ice-core measurements. From the elasticity tensors we derived seismic phase and group velocities of P-, SH- and SV-waves for cone, partial girdle and thick girdle structures, i.e. orthorhombic media. Velocities we derived for different cone fabrics agree well with velocities derived for cone fabric using the already established method of Bennett (1968). However, with our method it is now also possible to calculate velocities for girdle fabrics. Further, we can use the derived elasticity tensors to investigate the reflections coefficients in anisotropic ice.

We used the elasticity tensor to derive the reflection signature for englacial fabric changes and investigated the influence of anisotropic fabric on the reflection coefficients for basal reflectors. We found that the reflection coefficients and the variations of the reflection coefficients with increasing offset are weak for the transition between different COF distributions: They are at least an order of magnitude smaller than reflections from the ice–bed interface. Thus, either significant changes in the COF distribution or extremely sensitive measurement techniques are needed to observe englacial

seismic reflections. The influence of anisotropic ice fabric compared to the isotropic case for the reflection at the ice–bed interface is so small that it is within the measurement inaccuracy of currently employed seismic AVO analysis. An important result is that the difference between exact and approximate calculations of reflection coefficients for the ice–bed interface is larger than the influence of an anisotropic ice fabric above the bed. This implies that exact calculations are necessary if the fabric above the bed is in the focus of AVO analysis.

Better results in the calculation of the elasticity tensor could probably be gained by calculation of the opening angles directly from the c-axes vectors. This would avoid our classification into cone, partial girdle and thick girdle fabric. Nevertheless, the approach presented here offers the opportunity to use the readily available COF data from ice cores and go towards an investigation of the seismic wavefield in ice without the limitation to velocities only. The inclusion of further properties influencing the propagation of seismic waves in ice, like density and temperature, will offer the opportunity to model the complete wave field. Hence, we are confident that it will become feasible in the future to derive physical properties of the ice from analyses of the complete observed wave field by full waveform inversions.

Appendix A

From COF eigenvalues to elasticity tensor for seismics

600 A1 Connection of eigenvalues to opening angles

The following equations give the connection between the eigenvalues λ_1, λ_2 and λ_3 and the two opening angles φ and χ .

For a cone fabric the angle $\varphi = \chi$ is calculated by

$$\varphi = \chi = b_1 \sin(c_1 \lambda_3 + d_1) + b_2 \sin(c_2 \lambda_3 + d_2) + b_3 \sin(c_3 \lambda_3 + d_3) + b_4 \sin(c_4 \lambda_3 + d_4), \quad (\text{A1})$$

with

$$b_1 = 141.9, c_1 = 6.251, d_1 = 2.157,$$

$$b_2 = 139, c_2 = 10.33, d_2 = -1.809,$$

$$b_3 = 90.44, c_3 = 14.68, d_3 = 4.685,$$

$$610 \quad b_4 = 36.61, c_4 = 16.9, d_4 = 12.63.$$

For a thick girdle fabric the angle χ is calculated by

$$\chi = p_1 \lambda_1^7 + p_2 \lambda_1^6 + p_3 \lambda_1^5 + p_4 \lambda_1^4 + p_5 \lambda_1^3 + p_6 \lambda_1^2 + p_7 \lambda_1 + p_8, \quad (\text{A2})$$

$$615 \quad \varphi = 90^\circ, \quad (\text{A3})$$

with

$$p_1 = 2.957 \times 10^7, p_2 = -3.009 \times 10^7, p_3 = 1.233 \times 10^7, p_4 = -2.599 \times 10^6, \\ p_5 = 3.023 \times 10^5, p_6 = -1.965 \times 10^4, p_7 = 877.6, p_8 = 2.614.$$

620 For a partial girdle fabric the angle φ is calculated by

$$\varphi = a_1 \sin(b_1 \lambda_3 + c_1) + a_2 \sin(b_2 \lambda_3 + c_2) + a_3 \sin(b_3 \lambda_3 + c_3) + a_4 \sin(b_4 \lambda_3 + c_4), \quad (\text{A4})$$

$$\chi = 0^\circ, \quad (\text{A5})$$

with

$$625 \quad a_1 = 118.7, b_1 = 7.415, c_1 = -3.517,$$

$$a_2 = 97.47, b_2 = 13.68, c_2 = 1.161,$$

$$a_3 = 46.57, b_3 = 18.58, c_3 = 6.935,$$

$$a_4 = 7.455, b_4 = 25.18, c_4 = 11.47.$$

630 **A2 Rotation matrices for elasticity and compliance tensor**

Here the rotation matrix for the elasticity tensor and compliance tensor following Sunder and Wu (1994) are given. For the calculation of the elasticity tensor for different fabrics the monocrystal elasticity tensor needs to be rotated (Sect. 3.2).

The rotation matrix for the elasticity tensor is

$$635 \quad \mathbf{R}^C = \begin{pmatrix} l_1^2 & m_1^2 & n_1^2 & 2m_1nl_1 & 2n_1l_1 & 2l_1m_1 \\ l_2^2 & m_2^2 & n_2^2 & 2m_2nl_2 & 2n_2l_2 & 2l_2m_2 \\ l_3^2 & m_3^2 & n_3^2 & 2m_3nl_3 & 2n_3l_3 & 2l_3m_3 \\ l_2l_3 & m_2m_3 & n_2n_3 & m_2n_3 - m_3n_2 & n_2l_3 - n_3l_2 & l_2m_3 - l_3m_2 \\ l_3l_1 & m_3m_1 & n_3n_1 & m_3n_1 - m_1n_3 & n_3l_1 - n_1l_3 & l_3m_1 - l_1m_3 \\ l_1l_2 & m_1m_2 & n_1n_2 & m_1n_2 - m_2n_1 & n_1l_2 - n_2l_1 & l_1m_2 - l_2m_1 \end{pmatrix}, \quad (\text{A6})$$

and the compliance tensor

$$\mathbf{R}^S = \begin{pmatrix} l_1^2 & m_1^2 & n_1^2 & m_1nl_1 & n_1l_1 & l_1m_1 \\ l_2^2 & m_2^2 & n_2^2 & m_2nl_2 & n_2l_2 & l_2m_2 \\ l_3^2 & m_3^2 & n_3^2 & m_3nl_3 & n_3l_3 & l_3m_3 \\ 2l_2l_3 & 2m_2m_3 & 2n_2n_3 & m_2n_3 - m_3n_2 & n_2l_3 - n_3l_2 & l_2m_3 - l_3m_2 \\ 2l_3l_1 & 2m_3m_1 & 2n_3n_1 & m_3n_1 - m_1n_3 & n_3l_1 - n_1l_3 & l_3m_1 - l_1m_3 \\ 2l_1l_2 & 2m_1m_2 & 2n_1n_2 & m_1n_2 - m_2n_1 & n_1l_2 - n_2l_1 & l_1m_2 - l_2m_1 \end{pmatrix}, \quad (\text{A7})$$

640 with the following direction cosines

$$\begin{pmatrix} l_1 & l_2 & l_3 \\ m_1 & m_2 & m_3 \\ n_1 & n_2 & n_3 \end{pmatrix}, \quad (\text{A8})$$

for rotation around the x_1 -axis

$$645 \quad \begin{pmatrix} 1 & 0 & 0 \\ \cos \phi & -\sin \phi & 0 \\ \sin \phi & \cos \phi & 0 \end{pmatrix}, \quad (\text{A9})$$

for rotation around the x_2 -axis

$$\begin{pmatrix} \cos \phi & 0 & -\sin \phi \\ 0 & 1 & 0 \\ \sin \phi & 0 & \cos \phi \end{pmatrix}, \quad (\text{A10})$$

and for rotation around the x_3 -axis

$$650 \quad \begin{pmatrix} \cos \phi & -\sin \phi & 0 \\ \sin \phi & \cos \phi & 0 \\ 0 & 0 & 1 \end{pmatrix}. \quad (\text{A11})$$

A3 Components of elasticity and compliance tensor for polycrystal

The components of the polycrystal elasticity tensor as derived from Eq. (12) with c-axes distribution around the x_1 -axis, i.e. within the $[x_2, x_3]$ -plane are calculated by:

$$655 \quad \begin{aligned} C_{11}^p &= C_{11}^m, \\ C_{22}^p &= \frac{1}{2\phi_0} [b_1 C_{22}^m + b_2 C_{33}^m + 2b_3 (C_{23}^m + 2C_{44}^m)], \\ C_{33}^p &= \frac{1}{2\phi_0} [b_1 C_{33}^m + b_2 C_{22}^m + 2b_3 (C_{23}^m + 2C_{44}^m)], \\ C_{44}^p &= \frac{1}{2\phi_0} [(b_1 + b_2) C_{44}^m + b_3 (C_{22}^m - 2C_{23}^m + C_{33}^m - 2C_{44}^m)], \\ C_{55}^p &= \frac{1}{2\phi_0} [C_{55}^m (\phi_0 + \alpha) + C_{66}^m (\phi_0 - \alpha)], \\ 660 \quad C_{66}^p &= \frac{1}{2\phi_0} [C_{66}^m (\phi_0 + \alpha) + C_{55}^m (\phi_0 - \alpha)], \\ C_{12}^p &= \frac{1}{2\phi_0} [C_{12}^m (\phi_0 + \alpha) + C_{13}^m (\phi_0 - \alpha)], \\ C_{13}^p &= \frac{1}{2\phi_0} [C_{13}^m (\phi_0 + \alpha) + C_{12}^m (\phi_0 - \alpha)], \\ C_{23}^p &= \frac{1}{2\phi_0} [(b_1 + b_2) C_{23}^m + b_3 (C_{22}^m - 4C_{44}^m + C_{33}^m)]. \end{aligned} \quad (\text{A12})$$

665 The components of the polycrystal compliance tensor as derived from Eq. (13) with c-axes distribution around the x_1 -axis, i.e. within the $[x_2, x_3]$ -plane are calculated by:

$$\begin{aligned} S_{11}^p &= S_{11}^m, \\ S_{22}^p &= \frac{1}{2\phi_0} [b_1 S_{22}^m + b_2 S_{33}^m + b_3 (2S_{23}^m + S_{44}^m)], \end{aligned}$$

$$\begin{aligned}
S_{33}^p &= \frac{1}{2\phi_0} [b_1 S_{33}^m + b_2 S_{22}^m + b_3 (2S_{23}^m + S_{44}^m)], \\
670 \quad S_{44}^p &= \frac{1}{2\phi_0} \left[(b_1 + b_2) S_{44}^m + 4b_3 (S_{22}^m - 2S_{23}^m + S_{33}^m - \frac{1}{2} S_{44}^m) \right], \\
S_{55}^p &= \frac{1}{2\phi_0} [S_{55}^m (\phi_0 + \alpha) + S_{66}^m (\phi_0 - \alpha)], \\
S_{66}^p &= \frac{1}{2\phi_0} [S_{66}^m (\phi_0 + \alpha) + S_{55}^m (\phi_0 - \alpha)], \\
S_{12}^p &= \frac{1}{2\phi_0} [S_{12}^m (\phi_0 + \alpha) + S_{13}^m (\phi_0 - \alpha)], \\
S_{13}^p &= \frac{1}{2\phi_0} [S_{13}^m (\phi_0 + \alpha) + S_{12}^m (\phi_0 - \alpha)], \\
675 \quad S_{23}^p &= \frac{1}{2\phi_0} [(b_1 + b_2) S_{23}^m + b_3 (S_{22}^m - S_{44}^m + S_{33}^m)]. \tag{A13}
\end{aligned}$$

These variables apply for the equations for the calculation of the elasticity and compliance tensor of the polycrystal:

$$\begin{aligned}
b_1 &= \frac{3}{4} \phi_0 + \alpha + \beta, \\
680 \quad b_2 &= \frac{3}{4} \phi_0 - \alpha + \beta, \\
b_3 &= \frac{1}{4} \phi_0 - \beta, \\
\alpha &= \frac{1}{2} \sin 2\phi_0, \\
\beta &= \frac{1}{16} \sin 4\phi_0. \tag{A14}
\end{aligned}$$

$$685 \tag{A15}$$

Appendix B

Equations for calculation of velocities and reflection coefficients

B1 Velocities in anisotropic media

To be able to calculate velocities for partial girdle fabric the calculation of phase velocity for orthorhombic media derived by Daley and Krebs (2004) is used. They rearrange linearised equations to obtain the velocity from an ellipsoidal part with an ellipsoidal correction term:

$$v_p(\mathbf{n}) = \sqrt{1/\rho(C_{11}n_1^2 + C_{22}n_2^2 + C_{33}n_3^2 + 2B_{12}n_1^2n_2^2 + 2B_{13}n_1^2n_3^2 + 2B_{23}n_2^2n_3^2)}, \tag{B1}$$

$$v_{sv}(\mathbf{n}) = \sqrt{1/\rho(C_{44}\sin^2\psi + C_{55}\cos^2\psi + 2B_{12}n_1^2n_3^2\sin^2\psi - 2B_{13}n_2^2n_3^2 - 2B_{23}n_1^2n_3^2)}, \tag{B2}$$

$$695 \quad v_{sh}(\mathbf{n}) = \sqrt{1/\rho(C_{44}n_3^2\cos^2\psi + C_{55}n_3^2\sin^2\psi + C_{66}\sin^2\vartheta - 2B_{12}n_1^2\sin^2\psi)}, \tag{B3}$$

with

$$B_{12} = (C_{13} + 2C_{66}) - (C_{11} + C_{22})/2, \tag{B4}$$

$$B_{13} = (C_{12} + 2C_{55}) - (C_{11} + C_{33})/2, \quad (\text{B5})$$

$$700 \quad B_{23} = (C_{23} + 2C_{44}) - (C_{22} + C_{33})/2, \quad (\text{B6})$$

and the unit phase normal vector

$$\mathbf{n} = (n_1, n_2, n_3) = (\sin \vartheta \cos \psi, \sin \vartheta \sin \psi, \cos \vartheta). \quad (\text{B7})$$

with the phase angle ϑ and the azimuth ψ , here the azimuth for the orientation of a girdle fabric (Fig. 2).

705 The components of the group velocity vector are given by (Tsvankin, 2001)

$$v_{g,x_1} = v \sin \vartheta + \left. \frac{\partial v_{\text{ph}}}{\partial \vartheta} \right|_{\psi=\text{const}} \cos \vartheta, \quad (\text{B8})$$

$$v_{g,x_2} = \frac{1}{\sin \vartheta} \left. \frac{\partial v_{\text{ph}}}{\partial \psi} \right|_{\vartheta=\text{const}}, \quad (\text{B9})$$

$$v_{g,x_3} = v_{\text{ph}} \cos \vartheta + \left. \frac{\partial v_{\text{ph}}}{\partial \vartheta} \right|_{\psi=\text{const}} \sin \vartheta. \quad (\text{B10})$$

Within the symmetry planes the group velocity can be calculated using v_{g,x_1} and v_{g,x_2} only (Eq. (14))

710 Outside the symmetry planes of the HTI media the component v_{g,x_2} can not be neglected as the derivation $\frac{\partial v}{\partial \psi}$ is no longer zero. In this case v_g is the norm of the group velocity vector \mathbf{v}_g considering all three components v_{g,x_1} , v_{g,x_2} and v_{g,x_3} . Here, a second group angle (next to the one in the plane Eq. (15)) exists for the direction outside the plane with

$$\tan \theta_{\text{out}} = \frac{v_{g,x_2}}{\sqrt{v_{g,x_1}^2 + v_{g,x_3}^2}}. \quad (\text{B11})$$

715

B2 Reflection coefficients (Zillmer)

The reflection coefficients as derived by Zillmer et al. (1997, 1998a) are given by

$$R_{\text{PP}} = \frac{1}{4} \left(\frac{\Delta C_{33}}{C_{44}^{(0)} + 2C_{12}^{(0)}} + \frac{\Delta \rho}{\rho^{(0)}} \right) - \frac{1}{4} \frac{\Delta \rho}{\rho^{(0)}} \tan^2(\vartheta) + \frac{1}{4} \frac{2\Delta C_{13} - C_{33} - 4\Delta C_{55}}{C_{44}^{(0)} + 2C_{12}^{(0)}} \sin^2 \vartheta + \frac{1}{4} \frac{\Delta C_{11}}{C_{44}^{(0)} + 2C_{12}^{(0)}} \sin^2 \vartheta \tan^2 \vartheta, \quad (\text{B12})$$

$$720 \quad R_{\text{svsv}} = -\frac{1}{4} \left(\frac{\Delta C_{55}}{C_{12}^{(0)}} + \frac{\Delta \rho}{\rho^{(0)}} \right) - \frac{1}{4} \frac{\Delta \rho}{\rho^{(0)}} \tan^2(\vartheta) + \frac{1}{4} \frac{\Delta C_{11} - 2\Delta C_{13} + C_{33} - 3\Delta C_{55}}{C_{12}^{(0)}} \sin^2 \vartheta - \frac{1}{4} \frac{\Delta C_{55}}{C_{12}^{(0)}} \sin^2 \vartheta \tan^2 \vartheta, \quad (\text{B13})$$

$$R_{\text{shsh}} = -\frac{1}{4} \left(\frac{\Delta C_{44}}{C_{12}^{(0)}} + \frac{\Delta \rho}{\rho^{(0)}} \right) + \frac{1}{4} \left(\frac{\Delta C_{66}}{C_{12}^{(0)}} + \frac{\Delta \rho}{\rho^{(0)}} \right) \tan^2 \vartheta, \quad (\text{B14})$$

where Δ denotes the difference between the upper layer 1 and the lower layer 2, for example $\Delta C_{33} =$
725 $C_{33}^{(2)} - C_{33}^{(1)}$. The superscript (0) gives the isotropic reference values. When reflection coefficients

are calculated for different anisotropic ice fabrics, the density is constant, i.e. the $\Delta\rho$ -terms can be neglected ($\rho^{(2)} - \rho^{(1)} = 0$).

Acknowledgements. We thank T. Bohlen and his group of the Geophysical Institute, Karlsruhe Institute of Technology for their support and numerous hints during this study. Financial support for this study was provided to
730 O.E. by the Deutsche Forschungsgemeinschaft (DFG) "Emmy Noether"-program grant EI 672/5-1.

References

- Aki, K. and Richards, P. G.: Quantitative Seismology, University Science Books Sausalito, California, 2002.
- Anandakrishnan, S.: Dilatant till layer near the onset of streaming flow of Ice Stream C, West Antarctica, determined by AVO (amplitude vs offset) analysis, *Ann. Glaciol.*, 36, 283–286, 2003.
- 735 Ashby, M. F. and Duval, P.: The creep of polycrystalline ice, *Cold Reg. Sci. Technol.*, 11, 285–300, 1985.
- Bass, R., Rossberg, D., and Ziegler, G.: Die elastischen konstanten des Eises, *Zeitschr. f. Physik*, 149, 199–203, 1957.
- Bell, R. E., Ferraccioli, F., Creyts, T. T., Braaten, D., Corr, H., Das, I., Damaske, D., Frearson, N., Jordan, T., Rose, K., Studinger, M., and Wolovick, M.: Widespread Persistent Thickening of the East Antarctic Ice Sheet by Freezing from the Base, *Science*, 331, 1592–1595, doi:<http://dx.doi.org/10.1126/science.1200109>, 2011.
- 740 Bennett, H. F.: An investigation into velocity anisotropy through measurements of ultrasonic wave velocities in snow and ice cores from Greenland and Antarctica, Ph.D. thesis, University of Wisconsin-Madison, 1968.
- Bentley, C. R.: Seismic wave velocities in anisotropic ice: A comparison of measured and calculated values in and around the deep drill hole at Byrd Station, Antarctica, *J. Geophys. Res.*, 77, 4406–4420, 1972.
- 745 Blankenship, D. D. and Bentley, C. R.: The crystalline fabric of polar ice sheets inferred from seismic anisotropy, *The Physical Basis of Ice Sheet Modelling (Proceedings of the Vancouver Symposium)* IAHS Publ., pp. 54–57, 1987.
- Bower, A. F.: Applied mechanics of solids, CRC Press, Boca Raton, Fla., 2010.
- 750 Brockamp, B. and Querfurth, H.: Untersuchungen über die Elastizitätskonstanten von See- und Kunsteis, *Polarforschung*, 34, 253–262, 1964.
- Cuffey, K. M. and Paterson, W. S. B.: *The Physics of Glaciers*, Elsevier, 2010.
- Daley, P. and Heron, F.: Reflection and transmission coefficients for transversely isotropic media, *Bulletin of the Seismological Society America*, 67, 661–675, 1977.
- 755 Daley, P. F. and Krebes, E. S.: Alternative linearized expressions for qP, qS1 and qS2 phase velocities in a weakly anisotropic orthorhombic medium, *CREWES Research Report*, 16, 1–19, 2004.
- Dantl, G.: Die elastischen Moduln von Eis-Einkristallen, *Phys. kondens. Materie*, 7, 390–397, 1968.
- Diez, A.: Effects of cold glacier ice crystal anisotropy on seismic data, Ph.D. thesis, Karlsruhe Institute of Technology, Germany, 2013.
- 760 Diez, A., Eisen, O., Hofstede, C., Bohleber, P., and Polom, U.: Joint interpretation of explosive and vibroseismic surveys on cold firn for the investigation of ice properties, *Ann. Glaciol.*, 54, 201–210, 2013.
- Diez, A., Eisen, O., Weikusat, I., Hofstede, T. B. C., Lambrecht, A., Mayer, C., Miller, H., and Steinhage, D.: Seismic wave propagation in anisotropic ice: Part II. Inference of physical properties from geophysical data, *The Cryosphere*, 2014, *subm.*
- 765 Drews, R., Eisen, O., Weikusat, I., Kipfstuhl, S., Lambrecht, A., Steinhage, D., Wilhelms, F., and Miller, H.: Layer disturbances and the radio-echo free zone in ice sheets, *The Cryosphere*, 3, 195–203, doi:<http://dx.doi.org/10.5194/tc-3-195-2009>, 2009.
- Drews, R., Martin, C., Steinhage, D., and Eisen, O.: Characterizing the glaciological conditions at Halvfaryggen ice dome, Dronning Maud Land, Antarctica, *J. Glaciol.*, 59, 9–20, 2013.
- 770 Eisen, O., Hamann, I., Kipfstuhl, S., Steinhage, D., and Wilhelms, F.: Direct evidence for continuous radar

- reflector originating from changes in crystal-orientation fabric, *The Cryosphere*, 1, 1–10, <http://www.the-cryosphere.net/1/1/2007/>, 2007.
- Elvin, A. A.: Number of grains required to homogenize elastic properties of polycrystalline ice, *Mechanics of Materials*, 22, 51–64, 1996.
- 775 Faria, S. H., Weikusat, I., and Azuma, N.: The microstructure of polar ice. Part II: State of the art, *Journal of Structural Geology*, 61, 21–49, doi:<http://dx.doi.org/http://dx.doi.org/10.1016/j.jsg.2013.11.003><http://dx.doi.org/10.1016/j.jsg.2013.11.003>, 2014a.
- Faria, S. H., Weikusat, I., and Azuma, N.: The microstructure of polar ice. Part
780 I: Highlights from ice core research, *Journal of Structural Geology*, 61, 2–20, doi:<http://dx.doi.org/http://dx.doi.org/10.1016/j.jsg.2013.09.010><http://dx.doi.org/10.1016/j.jsg.2013.09.010>, 2014b.
- Fischer, H., Severinghaus, J., Brook, E., Wolff, E., Albert, M., Alemany, O., Arthern, R., Bentley, C., Blankenship, D., Chappellaz, J., Creyts, T., Dahl-Jensen, D., Dinn, M., Frezzotti, M., Fujita, S., Gallee,
785 H., Hindmarsh, R., Hudspeth, D., Jugie, G., Kawamura, K., Lipenkov, V., Miller, H., Mulvaney, R., Parrenin, F., Pattyn, F., Ritz, C., Schwander, J., Steinhage, D., van Ommen, T., and Wilhelms, F.: Where to find 1.5 million yr old ice for the IPICS "Oldest-Ice" ice core, *Climate of the Past*, 9, 2489–2505, doi:<http://dx.doi.org/10.5194/cp-9-2489-2013>[10.5194/cp-9-2489-2013](http://dx.doi.org/10.5194/cp-9-2489-2013), 2013.
- Fujita, S., Maeno, H., and Matsuoka, K.: Radio-wave depolarization and scattering within ice sheets: a matrix-
790 based model to link radar and ice-core measurements and its application, *J. Glaciol.*, 52, 407–424, 2006.
- Gammon, P. H., Kieft, H., Clouter, M. J., and Denner, W. W.: Elastic constant of artificial and natural ice samples by brillouin spectroscopy, *J. Glaciol.*, 29, 433–460, 1983.
- Graebner, M.: Plane-wave reflection and transmission coefficients for a transversely isotropic solid, *Geophysics*,
795 57, 1512–1519, doi:<http://dx.doi.org/10.1190/1.1443219>[10.1190/1.1443219](http://dx.doi.org/10.1190/1.1443219), 1992.
- Green, R. E. and Mackinnen, L.: Determination of the elastic constants of ice single crystals by ultrasonic pulse
method, *J. Acoust. Soc. Am.*, 28, 1292, 1956.
- Gusmeroli, A., Pettit, E. C., Kennedy, J. H., and Ritz, C.: The crystal fabric of ice from full-waveform borehole
sonic logging, *J. Geophys. Res.*, 117, F03 021, 2012.
- Hill, R.: The elastic behaviour of a crystalline aggregate, *Proc. Phys. Soc. A*, 65, 349–354, 1952.
- 800 Hofstede, C., Eisen, O., Diez, A., Jansen, D., Kristoffersen, Y., Lambrecht, A., and Mayer, C.: Investigating
englacial reflections with vibro- and explosive-seismic surveys at Halvfarryggen ice dome, Antarctica, *Ann.
Glaciol.*, 54, 189–200, 2013.
- Horgan, H. J., Anandakrishnan, S., Alley, R. B., Peters, L. E., Tsofias, G. P., Voigt,
D. E., and Winberry, J. P.: Complex fabric development revealed by englacial seismic
805 reflectivity: Jakobshavn Isbræ, Greenland, *Geophys. Res. Letters*, 35, L10 501+,
doi:<http://dx.doi.org/http://dx.doi.org/10.1029/2008GL033712><http://dx.doi.org/10.1029/2008GL033712>,
2008.
- Horgan, H. J., Anandakrishnan, S., Alley, R. B., Burkett, P. G., and Peters, L. E.: Englacial seismic reflectivity:
imaging crystal-orientation fabric in West Antarctica, *J. Glaciol.*, 57, 639–650, 2011.
- 810 Jona, F. and Scherrer, P.: Die elastischen Konstanten von Eis-Einkristallen, *Helvetica Physica Acta*, 25, 35–54,

1952.

Keith, C. M. and Crampin, S.: Seismic body waves in anisotropic media: reflection and refraction at a plane interface, *Geophys. J. R. astr. Soc.*, 49, 181–208, 1977.

Kohnen, H.: The temperature dependence of seismic waves in ice, *J. Glaciol.*, 13, 144–147, 1974.

815 Mainprice, D., Hielscher, R., and Schaeben, H.: Calculating anisotropic physical properties from texture data using the MTEX open-source package, Geological Society, London, Special Publications, 360, 175–192, doi:<http://dx.doi.org/10.1144/SP360.10>, <http://sp.lyellcollection.org/content/360/1/175.abstract>, 2011.

Martín, C., Gudmundsson, G. H., Pritchard, H. D., and Gagliardini, O.: On the effects of anisotropic rheology
820 on ice flow, internal structure, and the age-depth relationship at ice divides, *J. Geophys. Res.*, 114, 1–18, 2009a.

Martín, C., Hindmarsh, R. C. A., and Navarro, F. J.: On the effects of divide migration, along-ridge flow, and basal sliding on isochrones near an ice divide, *Journal of Geophysical Research: Earth Surface*, 114, F02006, doi:<http://dx.doi.org/10.1029/2008JF001025>, 2009b.

825 Matsuoka, K., Furukawa, T., Fujita, S., Maeno, H., Urantsuka, S., Naruse, R., and Watanabe, O.: Crystal orientation fabrics within the Antarctic ice sheet revealed by a mutlipolarization plane and dual-frequency radar survey, *J. Geophys. Res.*, 108, 2003.

Matsuoka, K., Wilen, L., Huerly, S. P., and Raymond, C. F.: Effects of birefringence within ice sheets on obliquely propagating radio waves, *IEEE Transactions on geoscience and remote sensing*, 47, 1429–1443,
830 2009.

Nanthikesan, S. and Sunder, S. S.: Anisotropic elasticity of polycrystalline ice Ih, *Cold Reg. Sci. Technol.*, 22, 149–169, 1994.

NEEM community members: Eemian interglacial reconstructed from a Greenland folded ice core, *Nature*, 493, 489–494, doi:<http://dx.doi.org/10.1038/nature11789>, 2013.

835 Penny, A. H. A.: A theoretical determination of the elastic constants of ice, *Mathematical Proceedings of the Cambridge Philosophical Society*, 44, 423–439, 1948.

Peternell, M., Hasalova, P., Wilson, C. J. L., Piazzolo, S., and Schulmann, K.: Evaluating quartz crystallographic preferred orientations and the role of deformation partitioning using EBSD and fabric analyser techniques, *Journal of Structural Geology*, 32, 803–817, 2010.

840 Peters, L. E., Anandakrishnan, S., Holland, C. W., Horgan, H. J., Blankenship, D. D., and Voigt, D. E.: Seismic detection of a subglacial lake near the South Pole, Antarctica, *Geophys. Res. Letters*, 35, L23501, doi:<http://dx.doi.org/10.1029/2008GL035704>, 2008.

Pettit, E. C., Thorsteinsson, T., Jacobson, H. P., and Waddington, E. D.: The role of crystal fabric in flow near an ice divide, *J. Glaciol.*, 53, 277–288,
845 doi:<http://dx.doi.org/doi:10.3189/172756507782202766>doi:10.3189/172756507782202766, 2007.

Polom, U., Hofstede, C., Diez, A., and Eisen, O.: First glacier-vibro seismic experiment—results from the cold firn of Colle Gniefitti, *Near Surface Geophysics*, 12, 493–504, doi:<http://dx.doi.org/10.3997/1873-0604.201305910>, 2014.

Raymond, C. F.: Deformation in the vicinity of ice divides, *J. Glaciol.*, 29, 357–373, 1983.

850 Reuss, A.: Berechnung der Fließgrenzen von Mischkristallen auf Grund der Platizitätsbedingung für

- Einkristalle, *Zeitschr. f. angew. Math. und Mech.*, 9, 49–58, 1929.
- Rommel, B. E. and Tsvankin, I.: Analytic description of P-wave ray direction and polarization in orthorhombic media, in: *Anisotropy 2000 : fractures, converted waves, and case studies*, edited by Ilkelle, L. T., pp. 1–19, Society of Exploration Geophysicists, 2000.
- 855 Rüger, A.: P-wave reflection coefficients for transversely isotropic models with vertical and horizontal axis of symmetry, *Geophysics*, 62, 713–722, 1997.
- Rüger, A.: *Reflection Coefficients and Azimuthal Avo Analysis in Anisotropic Media*, Geophysical Monograph Series, No. 10, Society of Exploration Geophysicists, 2002.
- Smith, A. M.: Subglacial bed properties from normal-incidence seismic reflection data, *J. Environ. Eng. Geophys.*, 12, 3–13, 2007.
- 860 Sunder, S. S. and Wu, M. S.: Crack nucleation due to elastic anisotropy in polycrystalline ice, *Cold Reg. Sci. Technol.*, 18, 29–47, 1994.
- Thomsen, L.: Weak anisotropic reflections, vol. 8 of *Offset-dependent reflectivity - Theory and Practice of AVO Analyses, Investigations in Geophysics Series*, Society of Exploration Geophysicists, 1993.
- 865 Tsvankin, I.: Seismic signatures and analysis of reflection data in anisotropic media, vol. 29 of *Handbook of geophysical exploration, seismic exploration*, Pergamon, 2001.
- Voigt, W.: *Lehrbuch der Kristallphysik: (mit Ausschluss der Kristalloptik)*, Bibliotheca mathematica Teubneriana ; 12, Johnson, New York, 1910.
- Wallbrecher, E.: *Tektonische und Gefügeanalytische Arbeitsweisen*, Ferdinand Enke Verlag, 1986.
- 870 Wilson, C. J. L., Russell-Head, D. S., and Sim, H. M.: The application of an automated fabric analyzer system to the textural evolution of folded ice layers in shear zones, *Ann. Glaciol.*, 37, 7–17, 2003.
- Woodcock, N. H.: Specification of fabric shapes using an eigenvalue method, *Geol. Soc. Am. Bull.*, 88, 1231–1236, 1977.
- Zillmer, M., Gajewski, D., and Kashtan, B. M.: Reflection coefficients for weak anisotropic media, *Geophys. J. Int.*, 129, 389–398, 1997.
- 875 Zillmer, M., Gajewski, D., and Kashtan, B. M.: Anisotropic reflection coefficients for a weak-contrast interface, *Geophys. J. Int.*, 132, 159–166, 1998a.
- Zillmer, M., Gajewski, D., and Kashtan, B. M.: Anisotropic reflection coefficients for a weak-contrast interface, *Geophys. J. Int.*, 132, 159–166, 1998b.

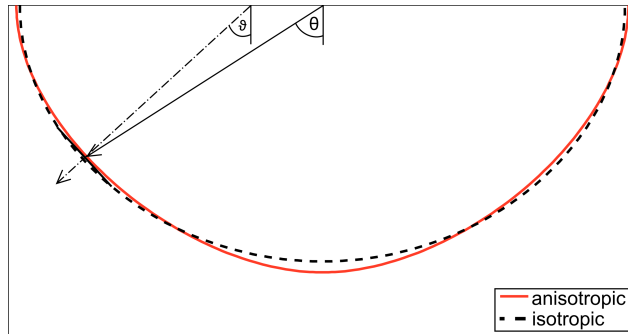


Fig. 1. Wavefront of a P-wave travelling in isotropic ice fabric (dashed line) and in a vertical single maximum (VSM) fabric (red line), thus, a vertical transversely isotropic (VTI) media. The solid arrow shows the group velocity with group angle θ , the dashed arrow the phase velocity with phase angle θ' for the anisotropic case.

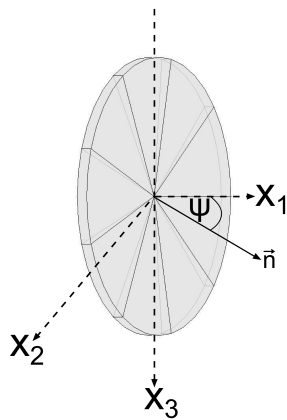


Fig. 2. Girdle fabrics classified as HTI media are within the $[x_2, x_3]$ -plane. If the girdle is rotated around the x_3 -axis the rotation is given by the azimuth ψ .

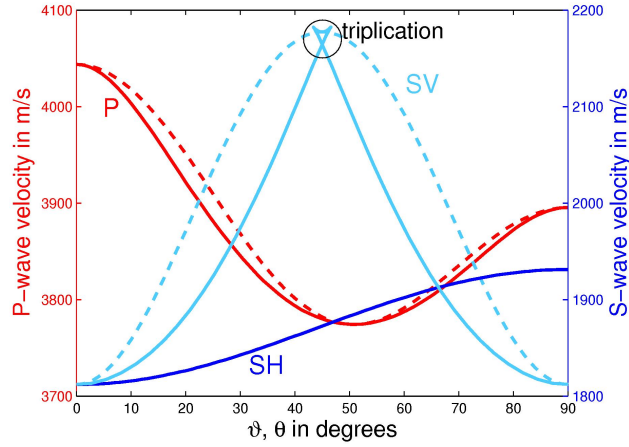


Fig. 3. Phase (dashed lines) and group velocities (solid lines) over the corresponding phase ϑ and group angle θ for P- (red curves), SH- (blue curves) and SV-waves (light blue curves) of a VSM-fabric. The SV-wave group velocity shows a triPLICATION for group angles θ between 43° and 46° .

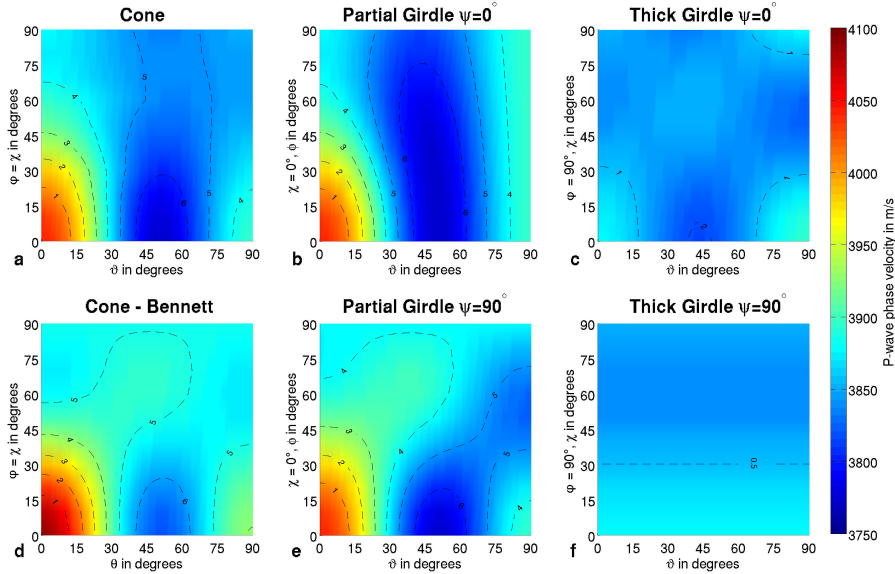


Fig. 4. P-wave phase velocities over phase angle ϑ for different fabrics. P-wave velocity for (a) different cone opening angles ($\varphi = \chi$), (b) partial girdle fabric ($\chi = 0^\circ$) and (c) thick girdle fabric ($\varphi = 90^\circ$) within the $[x_2, x_3]$ -plane, (e) partial girdle fabric ($\chi = 0^\circ$) and (f) thick girdle fabric ($\varphi = 90^\circ$) within the $[x_1, x_3]$ -plane calculated with equation (B1) given by Daley and Krebs (2004). (d) shows the P-wave velocity for different cone opening angles ($\varphi = \chi$) calculated with the equation given by Bennett (1968). The contour lines give the velocity differences in percent, in relation to the maximum velocity of the respective fabric group.

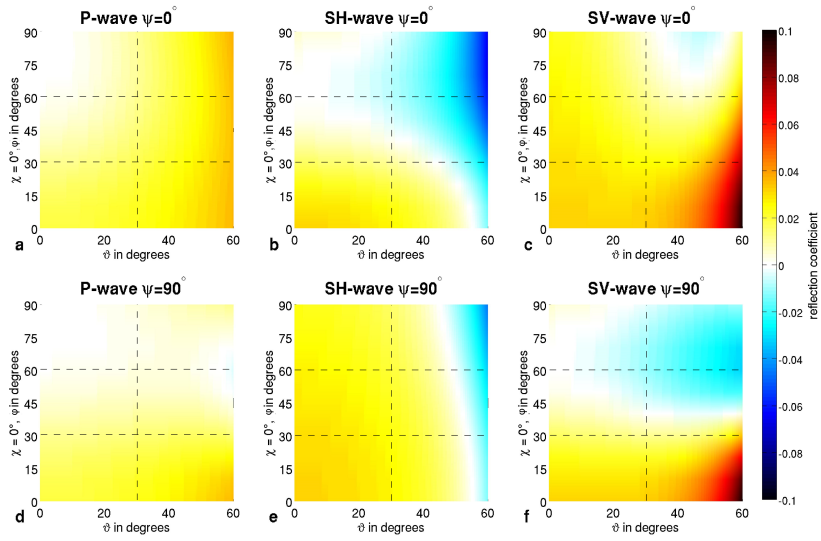


Fig. 5. Reflection coefficients for the boundary between an isotropic (upper) layer and a partial girdle fabric (lower) layer with different opening angles φ ($\chi = 0^\circ$) of the girdle. The reflection coefficients are calculated with equations given in Sect. 4.3 for different incoming phase angles ϑ . The subfigures (a), (b) and (c) show the reflection coefficients for a girdle orientation (lower layer) perpendicular to the travelpath of the wave (HTI media) for PP-, SHSH- and SVSV-reflection, respectively. The subfigures (d), (e) and (f) show the reflection coefficients for a girdle orientation parallel to the travelpath of the wave (azimuth $\psi = 90^\circ$) for PP-, SHSH- and SVSV-reflection, respectively.

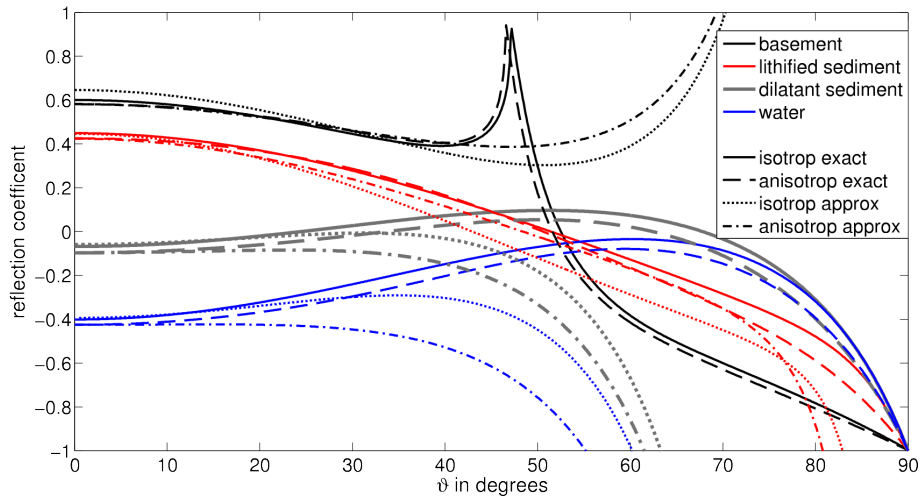


Fig. 6. P-wave reflection coefficients for ice–bed interface with different bed properties as a function of phase angle of incidence ϑ : basement (black), lithified sediments (red), dilatant sediments (gray) and water (blue). The solid and dotted lines are the reflection coefficients for an isotropic ice overburden, the dashed and dashed-dotted lines for the anisotropic (VSM) overburden. The solid and dashed lines are the reflection coefficients calculated with exact equations for VTI media given by Graebner (1992) and Ruger (2002). The dotted and dashed-dotted lines are approximate calculations following the approach by Aki and Richards (2002) for the isotropic case and that of Ruger (1997) for the anisotropic case, respectively. Property values for the bed and isotropic ice are taken from Peters et al. (2008). For the anisotropic ice the elasticity tensor given by Gammon et al. (1983) is used.

Table 1. The different ice crystal distributions as used for the calculation of seismic velocities and reflection coefficients. Given are the sketches for the enveloping of the c-axis distribution, the glaciological terms, the common stress regime and the corresponding eigenvalue range. In the second part the seismic term for the anisotropic regime is given together with the opening angles derived from the COF eigenvalues to calculate the elasticity tensor.

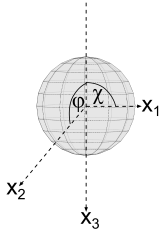
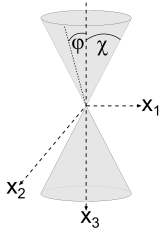
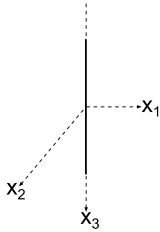
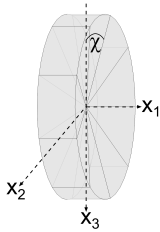
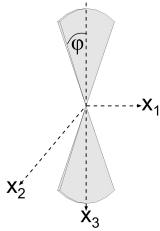
| fabrics envelope | glaciological context | | | seismic context | |
|---|-------------------------------------|---------------------------------------|---|--|---|
| | term | stress regime | eigenvalues | term | opening angle |
|  | isotropic | uniform | $\lambda_1 = \lambda_2 = \lambda_3 = 1/3$ | isotropic | $\varphi = \chi = 90^\circ$ |
|  | cone (cluster in mineralogy) | simple shear | $\lambda_1 = \lambda_2$ $\lambda_3 \geq \lambda_1, \lambda_2$ | vertical transversely isotropic (VTI) | $\varphi = \chi$ $0^\circ \leq \varphi \leq 90^\circ$ |
|  | vertical single maximum (VSM) | simple shear | $\lambda_1 = \lambda_2 = 0$ $\lambda_3 = 1$ | vertical transversely isotropic (VTI) | $\varphi = \chi = 0^\circ$ |
|  | thick girdle | uniaxial compression, extension | $\lambda_2 = \lambda_3$ $\lambda_1 = 1 - 2\lambda_2$ | horizontal transversely isotropic (HTI) | $\varphi = 90^\circ$ $0^\circ \leq \chi \leq 90^\circ$ |
|  | partial girdle | axial compression, extension | $\lambda_1 = 0$ $0 \leq \lambda_2 \leq 0.5$ $\lambda_3 = 1 - \lambda_2$ | orthorhombic | $\chi = 0^\circ$ $0^\circ \leq \varphi \leq 90^\circ$ |

Table 2. Steps for calculation of elasticity tensor (Eq. (13)) or compliance tensor (Eq. (13)) for different fabrics (Table 1).

| | step | rotation axis | angle |
|----------------|------|---------------|------------------|
| cone | 1 | x_1 | $\varphi = \chi$ |
| | 2 | x_3 | 90° |
| partial girdle | 1 | x_1 | φ |
| thick girdle | 1 | x_1 | 90° |
| | 2 | x_2 | χ |

Table 3. P-wave velocity, S-wave velocity and density for different bed scenarios and isotropic ice as given in Peters et al. (2008). These values are used for the calculation of reflection coefficients given in Fig. 6.

| material | v_p in m/s | v_s in m/s | ρ in kg/cm^3 |
|-------------------|--------------|--------------|-----------------------------------|
| ice | 3810 | 1860 | 920 |
| basement | 5200 | 2800 | 2700 |
| lithfied sediment | 3750 | 2450 | 2450 |
| dilatant sediment | 1700 | 200 | 1800 |
| water | 1498 | 0 | 1000 |